Psychophysiology, 41 (2004), 313–325. Blackwell Publishing Inc. Printed in the USA.

DOI: 10.1046/j.1469-8986.2003.00141.x

Automatic removal of eye movement and blink artifacts from EEG data using blind component separation

CARRIE A. JOYCE,[a] IRINA F. GORODNITSKY,[b] AND MARTA KUTAS[b,c]

[a]Department of Computer Science, University of California–San Diego, La Jolla, California, USA
[b]Department of Cognitive Science, University of California–San Diego, La Jolla, California, USA
[c]Department of Neurosciences, University of California–San Diego, La Jolla, California, USA

Abstract

Signals from eye movements and blinks can be orders of magnitude larger than brain-generated electrical potentials and are one of the main sources of artifacts in electroencephalographic (EEG) data. Rejecting contaminated trials causes substantial data loss, and restricting eye movements/blinks limits the experimental designs possible and may impact the cognitive processes under investigation. This article presents a method based on blind source separation (BSS) for automatic removal of electroocular artifacts from EEG data. BBS is a signal-processing methodology that includes independent component analysis (ICA). In contrast to previously explored ICA-based methods for artifact removal, this method is automated. Moreover, the BSS algorithm described herein can isolate correlated electroocular components with a high degree of accuracy. Although the focus is on eliminating ocular artifacts in EEG data, the approach can be extended to other sources of EEG contamination such as cardiac signals, environmental noise, and electrode drift, and adapted for use with magnetoencephalographic (MEG) data, a magnetic correlate of EEG.

Descriptors: Electroencephalogram, Artifact, Electrooculogram, Automated, Blind source separation, Independent component analysis

Eye movements and blink contamination are pervasive problems in event-related potential (ERP) research. The electric potentials created during saccades and blinks can be orders of magnitude larger than the electroencephalogram (EEG) and can propagate across much of the scalp, masking and distorting brain signals. This report describes a novel, robust, completely *automated* method for eliminating electroocular contamination from EEG signals using statistical criteria applied to data components obtained using a blind source separation (BSS) algorithm. The principles of this method can be extended to certain other sources of artifacts as well. To our knowledge, no automated BSS-based methods correcting for ocular artifacts in EEG data have been developed with the exception of a semiautomated method by Delorme, Makeig, and Sejnowski (2001). Automated methods are preferable because they eliminate the subjectivity associated with nonautomated correction, are significantly more time and resource efficient, and can make it practical to use such applications during on-line EEG monitoring for clinical and other uses. Ocular artifacts are nontrivial to measure and model in part because they are generated by two (or more) distinct mechanisms that induce very different propagation patterns across the scalp. Blink artifacts are attributed to alterations in conductance arising from contact of the eyelid with the cornea (Overton & Shagaas, 1969). An eyeblink can last from 200 to 400 ms and can have an electrical magnitude more than 10 times that of cortical signals. The majority of this signal propagates through the superficial layer of the face and head and decreases rapidly with distance from the eyes. Eye movements generate another type of electric signal. The cornea of the eye is positively charged relative to the retina, which amounts to having a steady retino-corneal charge of between 0.4 and 1.0 mV that approximates a dipole in both eyes. As the retino-corneal axis rotates during eye movements, the orientation of this dipole in three-dimensional space also rotates, resulting in changes in electric potential. The signals due to eye movement propagate mainly through the shunt pathway provided by the eye sockets. These signals attenuate more slowly than blink signals, but because the latter tend to generate much larger electrical amplitudes, both ocular artifacts have extensive spread, reaching even occipital electrode sites.

Some of the methods devised for dealing with ocular artifacts seek to minimize their presence by restricting eye movements and blinking during data collection or by excluding artifact-contaminated trials from the analyzed data. Other methods seek to correct for ocular artifacts in the data; these include subtraction or regression in the time or frequency domain (see Gratton, 1998, for a review) and methods that model the electrooculogram (EOG) components to isolate them from the

I.F.G. was supported by a grant from NSF (IIS-0082119). C.A.J. and M.K. were supported by grants from the McDonnell Foundation (15573-S6), NICHD (22614), and NIA (08313).

Address reprint requests to: Marta Kutas, Department of Cognitive Science, University of California–San Diego, La Jolla, CA 92093-0114, USA. E-mail: mkutas@ucsd.edu.

brain signals (see Lins, Picton, Berg, & Scherg, 1993a, 1993b, for an evaluation). With very few exceptions, the latter methods (i.e., modeling) use either: (1) localization (source modeling/imaging) of active generators of recorded data (e.g., Berg and Scherg, 1991a) or (2) decomposition of scalp data into underlying components (component modeling) with the idea of capturing the independent processes that contribute to the scalp recordings. The localization methods model EOG generators as dipoles and subtract their contribution from the EEG data. This approach is tantamount to learning the locations of electrically active sources inside and outside the brain at a given time. The general nonuniqueness of source localization solutions and the poor spatial resolution afforded by EEG data, particularly if sources are closely spaced (e.g., Achim, Richer, & Saint-Hilaire, 1991), are two well-known issues that limit applicability of this approach. Another limiting factor is the nontrivial propagation of EEG and EOG signals across the head and scalp, which means that the distribution of the tissues in the head must be known precisely to model this propagation accurately throughout the head.

Decomposition methods identify individual signal components in EEG data without reference to head or source propagation models, so they are not subject to the above constraints. EEG component separation procedures using principal components analysis (PCA) and its counterpart, singular value decomposition (SVD) were proposed by Berg and Scherg (1991b) and Sadasivan and Dutt (1996), among others. By definition, PCA and SVD assume that the data components are algebraically orthogonal, a condition that, in general, is hard to satisfy. The actual algebraic relationship between source vectors is a function of each source location, orientation, and to some degree the head conductance parameters. Orientation of certain ocular generators (e.g., blinks) may even be nearly aligned with orientation of frontal EEG generators. A more advanced method (Berg & Scherg, 1994) that combines source modeling, PCA, and artifact averaging provides an improvement on the individual techniques above but requires a substantial amount of calibration data and prior modeling of artifact production and event-related activities. More recently, Vigario (1997), Jung et al., (2000), and a number of other researchers have turned to ICA for finding components of EEG/EOG data. ICA aims to project (decompose) data onto statistically independent components utilizing higher-order statistical measures, beyond the second-order statistics used by PCA. These methods represent a subclass of the general group of blind source separation (BSS) algorithms.

An independent component analysis (ICA)-based method for removing artifacts semiautomatically was presented in Delorme et al. (2001). Although it is automated to flag trials as potentially contaminated, these trials are still examined and rejected manually via a graphical interface. The method is designed to eliminate all types of artifacts by considering them as "odd" data points, using statistical criteria—probability distribution and kurtosis—to measure trial "oddness." There are several differences between this approach and the one proposed herein. First, the motivation for the current procedure is different, as it comes out of an interest in studies where eye movements are an integral part of an experiment rather than an unexpected event. Using measures to identify trial oddness would not be appropriate in this case. Second, the current approach seeks to correct optimally for one particular artifact, rather than to reject many different types of artifacts via a single procedure. With this goal in mind, the method is tuned to exploit the particulars of ocular signals, achieving sufficient accuracy to allow for a completely automated artifact correction. Third, the current procedure teases out the EOG from EEG rather than rejecting artifact-contaminated trials. Last but not least, the current procedure does not use ICA but a BSS approach called second order blind inference (SOBI; Belouchrani, Abed-Meraim, Cardoso, & Moulines, 1997), which uses decorrelation across seveal time points as its basic computational step. This seemingly simple approach has proven very powerful in separating EEG from EOG sources.

One may wonder why component-modeling methods are not subject to the same poor spatial resolution from EEG data as are source localization methods. One chief reason is that component modeling does not require models of signal propagation across the scalp, thus eliminating a large source of inaccuracy in source estimation. Another reason is the difference in how the data are utilized by BSS compared to the source localization algorithms. BSS uses statistical relationships between the electrical signals (components) to identify them. Thus, closely spaced neural/ocular activities with different temporal dynamics can be identified as physiologically separate processes by virtue of the statistical properties of the components generated by the processes. Finally, BBS method outputs do not identify the absolute source head locations, only their relative positions with respect to other sources, which is a simpler problem to solve. Thus, it does not generate the same errors when data resolution is limited.

Methods

Developing a practical optimized method requires consideration of issues beyond the algorithm itself. Issues concerning how to best register and prefilter ocular signals are described first, followed by a discussion of the SOBI algorithm and the procedure for automated classification of artifacts. Each step is illustrated by an example using data recorded from 15 scalp and 6 EOG electrodes, referenced on-line to the left mastoid, and sampled at 500 Hz with an on-line bandpass filter from 0.016 to 100 Hz.

Practical Design Issues

EOG electrode placement. Good sampling of eye-generated signals is essential for separating out the ocular artifacts in EEG data. Generally, two horizontal (one left, one right) and two vertical (one upper, one lower) electrodes are sufficient to get good separation of the eye-movement-related components (Joyce, Gorodnitsky, King, & Kutas, 2002). Figure 1 (column 2) shows that, when using only one horizontal and one vertical electrode, the method leaves residual EOG noise in the corrected data whereas using two horizontal and two vertical electrodes (one upper, one lower for one eye) yields better results (column 3). Adding upper and lower electrodes to the other eye does little to improve the correction over the four-electrode case (column 4).

The issues of electrode placement and referencing are closely linked. In many cases, separation using monopolar (referenced to a common electrode, e.g., mastoid) and bipolar (upper referenced to lower, left referenced to right electrodes) EOG yields similar solutions. For this method, however, monopolar

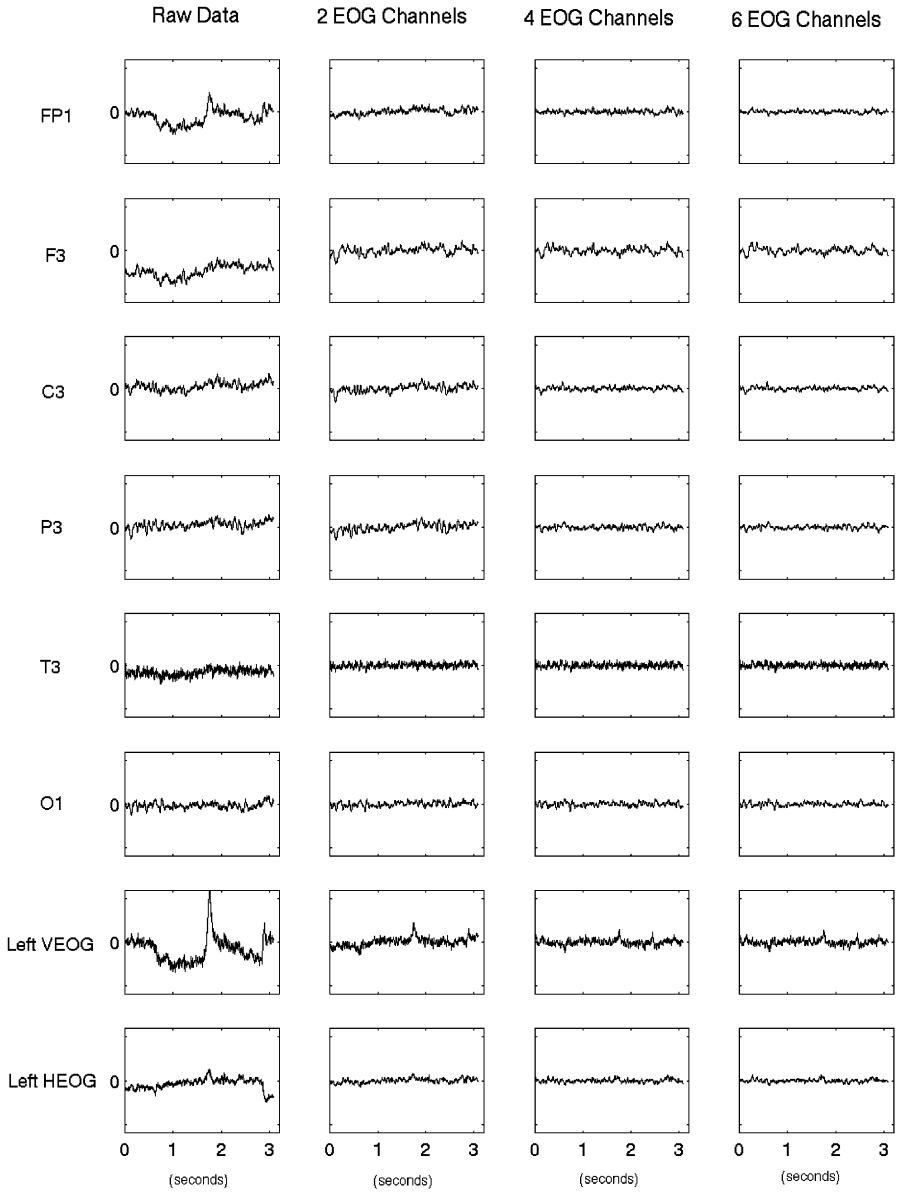

Figure 1. Column one shows raw data and columns two through four show BSS-corrected data using two, four, and six EOG channels, respectively. Note especially in the left VEOG channel, the remaining blink contamination with only two EOG electrodes, whereas this is much reduced for both four and six EOG electrodes. The solutions for four and six electrodes are virtually identical.

EOG recordings are essential for automating the procedure. In general, monopolar EOG data are preferable in ocular artifact detection routines because any misalignments between the cross-referenced electrodes in bipolar recordings may introduce offsets, essentially slow drifts, into the data. Figure 2 illustrates that better separation and correction are obtained with monopolar EOG recordings when eye-related drift is present in the recorded signal. As stated above, the monopolar recordings shown in Figure 2 are referenced to left mastoid.

Correction for instrument response artifacts. The key to applying BSS to the problem of finding data components is consistent registration of signals across all sensors. Two issues arise with respect to fulfilling this requirement. One is the need for a common gain scale. A frequent practice when recording EEG data is to adjust the gain on some channels, particularly those around the eyes and over frontal areas, where large signals might exceed the maximum parameters of the circuit, resulting in data loss and/or distortion. Without such a gain adjustment, the amplitude of the blink signal would be largest at the EOG and frontal electrodes, diminishing with distance from the eyes. However, adjusting the gain on these electrodes to avoid blocking distorts the relative size of the ocular signals across the channels. Therefore, gain must be normalized across all channels prior to submitting the data to any artifact detection/correction algorithms.

The second issue is relevant to those using many of the common types of AC amplifiers to record EEG signals. Slow eye movements induce near-DC signals that register with some attenuation factor at electrodes across the scalp. Many AC

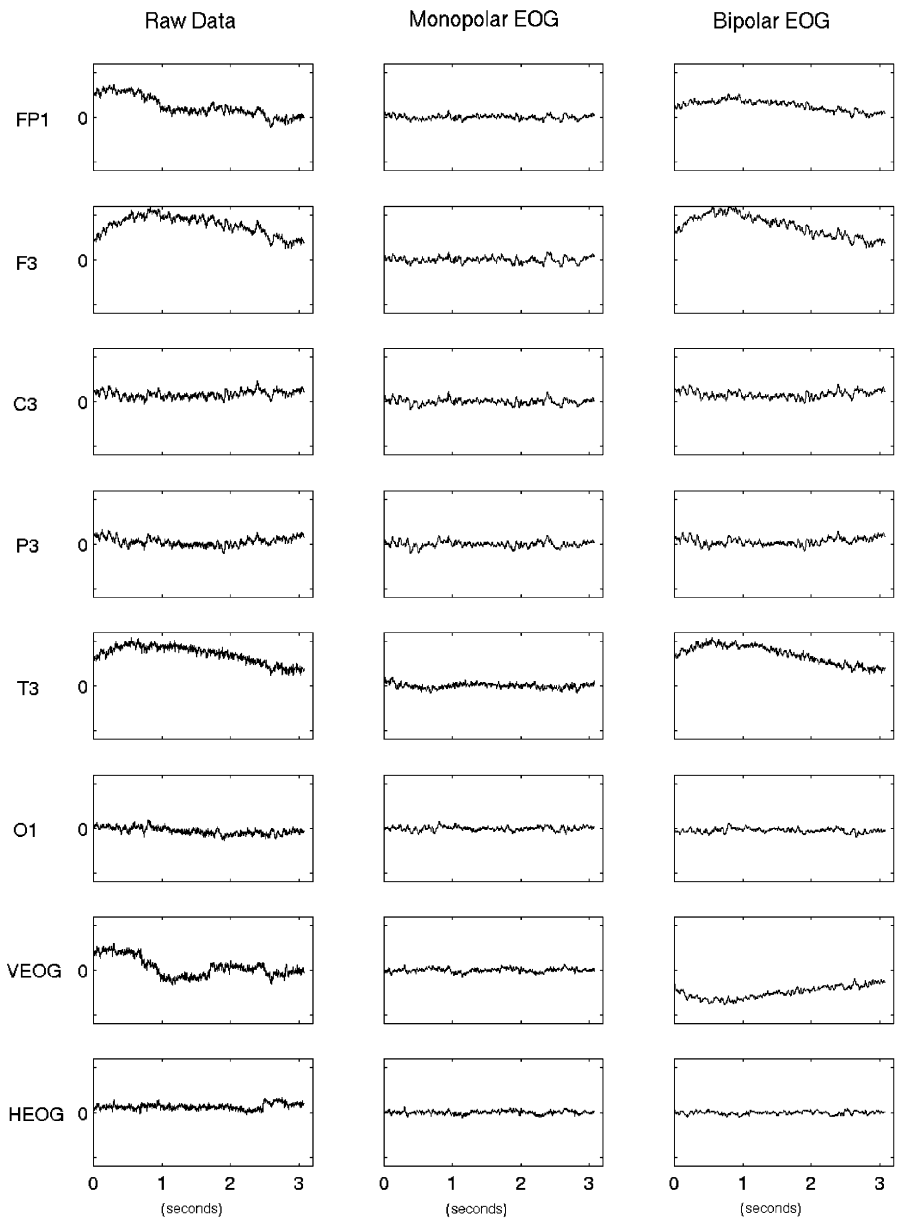

Figure 2. Column one shows raw data and columns two and three show BSS-corrected data for monopolar and bipolar EOG, respectively. The drift signal present in the raw vertical data is corrected out when using monopolar but not bipolar referenced EOG electrodes.

amplifiers used in EEG research distort the DC and near DC components. The distortions are in the form of a drift that can be observed in any channel that registers slowly changing components. Moreover, technically identical AC amplifier circuits housed in different amplifier channels may distort DC signals at different rates. The problem is thus akin to the channel normalization issue in the sense that instrument response is not identical across channels. This is an important but underappreciated point. One cannot count on removing the AC bias simply by finding its component in the data; it must be corrected on a channel-by-channel basis.

The effect of uneven gains and distortions across electrodes is tantamount to "shifting" the position of origin of the ocular signals away from the eyes toward anterior channels, such that the ocular component may be estimated incorrectly. To remedy this problem, responses of the individual channels must be equalized. Gain normalization is fairly standard and can be found in most EEG processing software. The channels are simply scaled proportional to the magnitude of square wave calibration pulses measured for each channel. The AC amplifier distortions, on the other hand, are not simple to rectify because amplifier responses can be quite different from their technical specifications and can vary across channels for amplifiers of identical make. Joyce, Gorodnitsky, Teder-Sälejärvi, King, and Kutas (2002) recently presented one method for correcting AC-related distortions. The description of the method is somewhat lengthy and the reader is referred to that paper for further details.

Note that the problem with AC amplifiers cannot be circumvented by using DC amplifiers for EOG channels and AC amplifiers for EEG, because DC distortions will register

across many EEG channels. To the extent that the AC amplifiers generate a bias, it will distort data in those channels. To make instrument response as consistent as possible across all channels, one must use the same type of amplifier for both the EEG and EOG recordings.

A separate issue from the ones just described is that slow drifts can leak into data from the reference channel. This artifact, however, is consistent across channels and can be removed by identifying the common component via BSS decomposition. The procedure presented here uses this method to remove this bias.

Blind Source Separation

The raw scalp data represent a projection of a set of signals, which are a mix of brain and artifact information, onto the electrode sites. Blind separation reduces mixtures of neural and nonneural variables to components that are in some way independent of each other. Different ways of measuring independence give rise to different BSS algorithms.

The idea behind BSS analysis is to produce components that correspond to distinct neural and nonneural activity, for example, an externally generated noise or an ocular artifact. These components are found without using signal propagation/head models: The data are "blindly" processed. The advantage of this is that BSS algorithms are not affected by errors in head propagation models. The disadvantage is that there is no guarantee that any particular BSS method can capture the individual signals in its components.

Component estimation from EEG data is formulated as follows. Electromagnetic waves throughout the head combine linearly to produce the total current measured at the scalp. Accordingly, unmixing scalp data into components can be done through a linear rotation (projection). This is written in a mathematical form as follows:

$$\mathbf{S} = \mathbf{W} * \mathbf{D}, \tag{1}$$

meaning that the sensor data $\mathbf{D}$ is rotated by an unmixing matrix $\mathbf{W}$ to arrive at the components $\mathbf{S}$. To clarify, all quantities in Equation 1 are matrices. The inverse, $\mathbf{W}^{-1}$, is referred to as the mixing matrix, each column of which describes signal propagation from an individual source to each electrode site. Thus $\mathbf{W}^{-1}$ is similar to the forward model of source imaging methods.

Given that nothing except the data, $\mathbf{D}$, is known in Equation 1, assumptions about the signals (components) must be made in order to define the unmixing matrix, $\mathbf{W}$. The difference among various BSS methods is in how each measures the independence between the components. This, in turn, defines the matrix, $\mathbf{W}$, and the components that are obtained. ICA algorithms assume that the components are statistically independent at each time point and use higher (e.g., fourth) order (spatial) moments of data in their estimation. The relationships across time (i.e., between component values at different time lags) are not considered by ICA algorithms.

The SOBI algorithm used in the current analysis is based on a different set of assumptions and thus produces different data components. SOBI considers the relationship between component values at different time lags and insists that these values be decorrelated as much as possible. Note that they cannot be decorrelated completely because a perfect zeroing of data cross-correlations at several time lags simultaneously with a single rotation matrix is mathematically impossible. This defines a major strength of SOBI: Its remaining correlated components can isolate highly temporally correlated sources (Belouchrani, Abed-Meraim, Cardoso, & Moulines, 1993), something that most ICA algorithms cannot do.

Mathematically, the matrix of the cross-correlations of sensor data at time lag τ can be written as

$$\mathbf{R}(\tau) = \mathbf{E}[\mathbf{x}(\mathbf{t})\mathbf{x}(\mathbf{t}-\tau)'], \tag{2}$$

where $\mathbf{E}[\ ]$ is the expectation operator. The cross-correlation terms at time delay τ are contained in the off-diagonal terms of this matrix. The unmixing matrix, $\mathbf{W}$, in SOBI is computed as the matrix that jointly diagonalizes a set of $\boldsymbol{p}$ whitened cross-correlations matrices $\{\mathbf{R}_{\mathbf{W}}(\tau_i)|\ i = 1, \ldots, p\}$. Hence the projection axes in SOBI are constrained by a statistic that is averaged in two separate ways over time: One average occurs when the cross-correlation of sensor data at a fixed delay is used, and the second when an aggregate metric of several delays is used.

SOBI's ability to resolve correlated activity is a crucial feature for ocular artifact detection because the ocular movement signals coming from the two eyes are highly correlated. More importantly, these signals can be highly correlated with frontal activity and signals coming from the parietal area that are related to motion control. A validation study of correlated EEG/EOG component separation was performed using data described in Gorodnitsky and Belouchrani (2001) in which the authors used carefully calibrated eye motion recordings to evaluate ocular artifact components obtained from various BSS/ICA algorithms. The results of the complete study are still in preparation, but in brief, the authors test three popular ICA algorithms: extended Infomax (Lee, Girolami, & Sejnowski, 1999), fICA (Hyvarinen & Oja, 1997), and JADE (Cardoso & Souloumiac, 1993), in addition to SOBI. They find only SOBI capable of successfully identifying, in a consistent manner across many different sets of data, the highly temporally correlated components generated by the two eyes moving in unison, in addition to what appear to be components of frontal and nonfrontal brain activity correlated with ocular motion.

Clearly, it is difficult to evaluate the quality of various BSS solutions given the inability to directly measure the individual electric signals that comprise the EEG data. In this situation, it is prudent to choose the BSS algorithm whose assumptions most closely fit the properties of the physical problem at hand. The algorithms that do not provide a close fit unavoidably will lead to components that do not match the actual EEG/EOG sources. Besides its ability to separate correlated activities, SOBI has very lenient requirements regarding the data and their sources. Such considerations in conjunction with empirical validations similar to one described in Gorodnitsky and Belouchrani (2001) identified SOBI as the best algorithm for this particular analysis. SOBI was also independently selected by Tang, Pearlmutter, Malaszenki, Phung, and Reeb (2002) to find components of cognitive activity, which typically generates weak signals, in a magnetoencephalography (MEG) study.

A considerable number of ICA based EEG/EOG analyses have been published to date, but not necessarily with sufficient background to enable an EEG practitioner to choose among the different algorithms. Given the importance that the algorithms' underlying assumptions have on solution quality, some background material on BSS is presented in the Discussion.

Note that the present discussion does not mean to imply that SOBI is the overall best approach for decomposing EEG sensor data into meaningful components. At the time this study was conducted, SOBI offered the best performance among the existing BSS (ICA) algorithms for this specific application. Further improvements to BSS methods for EEG analysis are

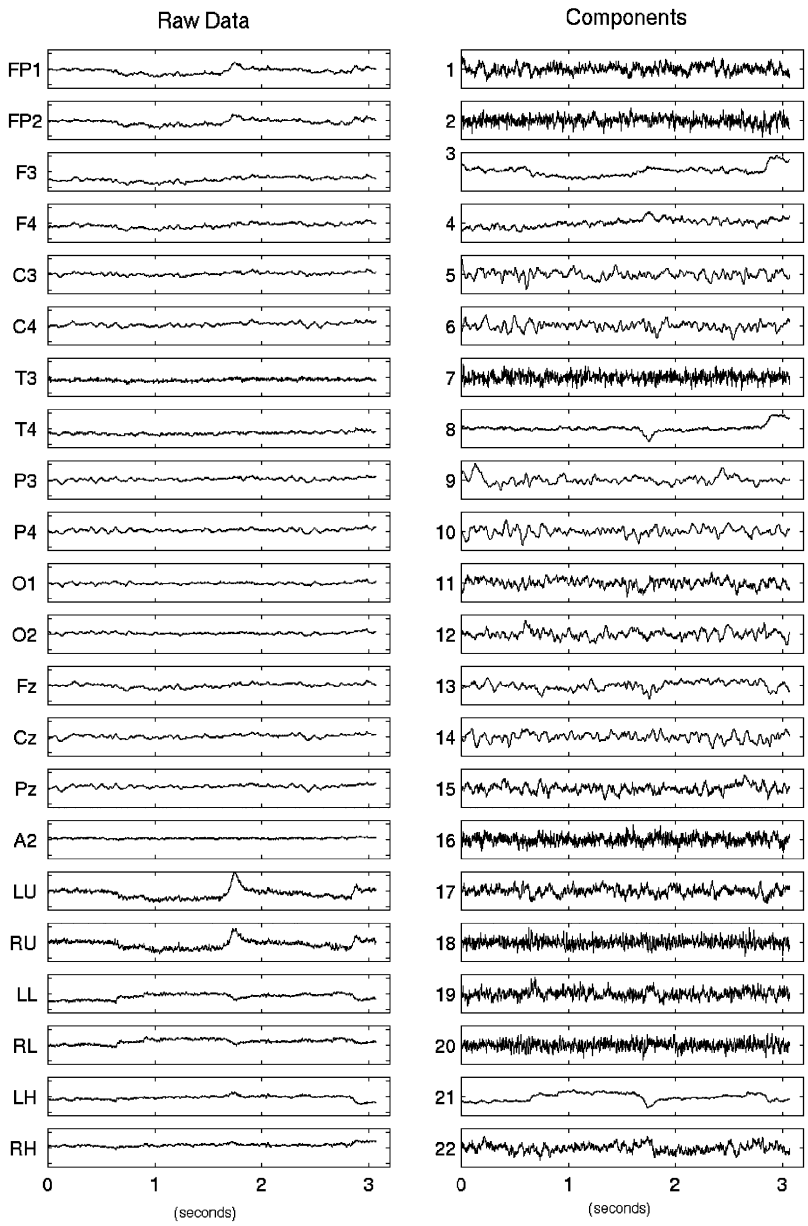

Figure 3. Column one shows preprocessed data at all recorded sites (15 EEG, 1 mastoid, 6 EOG). Column two shows the components extracted using SOBI.

possible and clearly needed. As improvements are made in algorithms for EEG analysis, a BSS algorithm of choice can be substituted easily in the automated procedure described herein.

Results

Automated Isolation and Removal of Ocular Components

Before describing the step-by-step automated ocular artifact correction method, it is worth noting that a simpler way to correct for artifacts may be possible in the future if algorithms can be developed which consistently and with high precision extract the pure components of ocular activity. Then the signals originating from the eyes can be identified from those components and removed from the EEG data by nulling the columns of the matrix $\mathbf{W}^{-1}$ in Equation 1 that correspond to the ocular sources. In an ideal BSS decomposition, each column of $\mathbf{W}^{-1}$ represents a forwardly modeled dipole (active source). The forward model, which can be described by the linear Poisson equation, describes the geometric relationship between the dipole and the electrode positions. The absolute dipole (source) locations can then be obtained from the $\mathbf{W}^{-1}$ column values in conjunction with the estimated signal amplitudes by applying certain additional geometric considerations.

As it stands now, the BSS methods cannot yet be trusted to consistently identify pure individual signal components. Even though SOBI separates the ocular activity quite cleanly from the rest of the data components, small amounts of leakage between the ocular and nonocular components can occur, and the ocular sources also may be represented in several components each reflecting some part of the eye motion. As a result, a geometric mapping of the components would reveal a distribution of

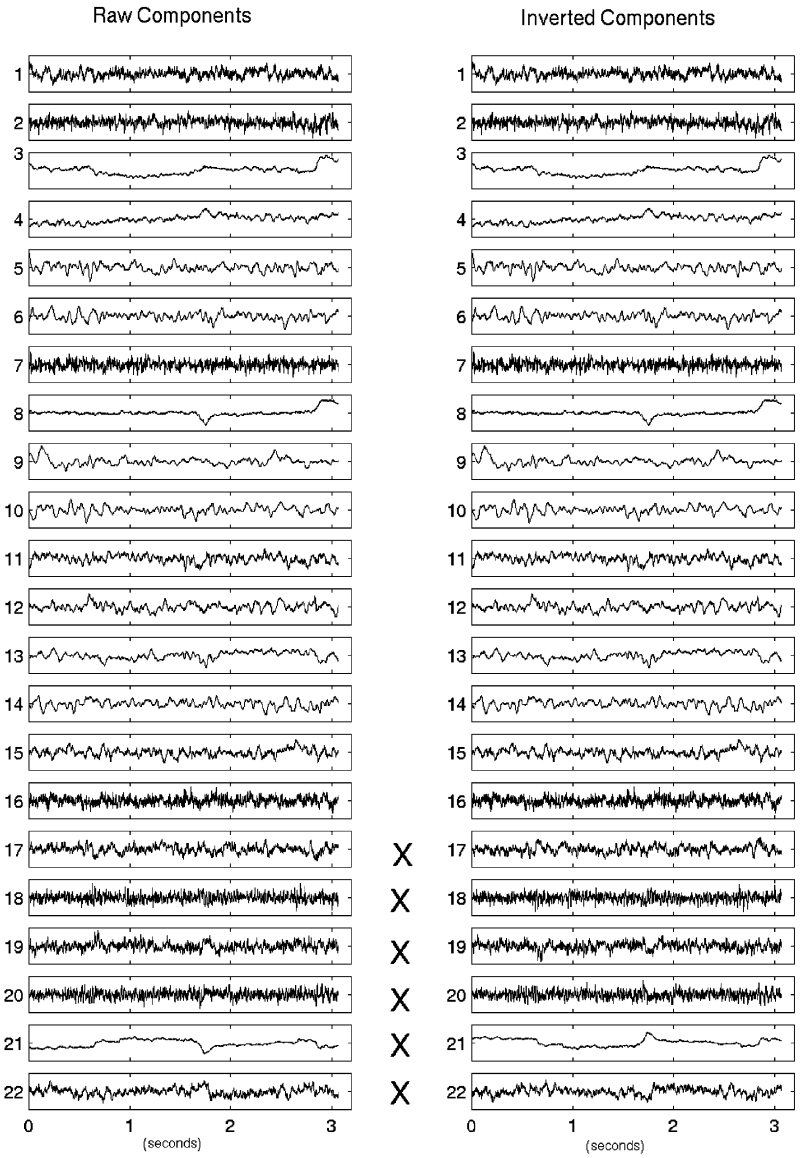

Figure 4. Column one show the components extracted by SOBI from the preprocessed data. Column two shows the components extracted by SOBI from the inverted EOG data. Xs denote components that "flipped" due to the EOG channel inversion and are marked for elimination.

sources that fall in the vicinity of the eyes, rather then on the eyes themselves. This can give rise to uncertainty as to which components are frontal and which are ocular. The method described here identifies the artifact signals using an alternative approach: a novel data reversal step and a cross-correlation test. It is important to understand here that there is no claim that the components found contain pure ocular and brain signals. However, the majority of the ocular signal power can be identified and extracted, leaving relatively minor noise in the data. For most EEG/ERP studies involving identification of gross brain responses (e.g., evoked responses), the accuracy provided by the present method should be quite good.

The automated procedure for extracting and removing ocular components can be broken down into five steps, as follows:

1. Decompose the data onto a set of components (i.e., rotate to new axes) using a BSS algorithm.
2. Reverse the sign on all lower and horizontal EOG channels (i.e., multiply signals by -1) and again decompose data onto components using a BSS algorithm. Flag those components that invert.
3. Flag BSS components that correlate above a certain level with the preprocessed lower and horizontal EOG channel data.
4. Flag BSS components with high power in the low frequency band.
5. Remove from the data those components identified in Step 2, and those that were identified in both Steps 3 and 4.

Step 1. Figure 3 illustrates the first step of the procedure where SOBI is applied to one trial of preprocessed EEG/EOG data. BSS methods determine component waveshapes uniquely up to an arbitrary scale factor, giving the user freedom to choose a consistent scaling convention. In this implementation, SOBI normalizes the component amplitudes (i.e., each component is

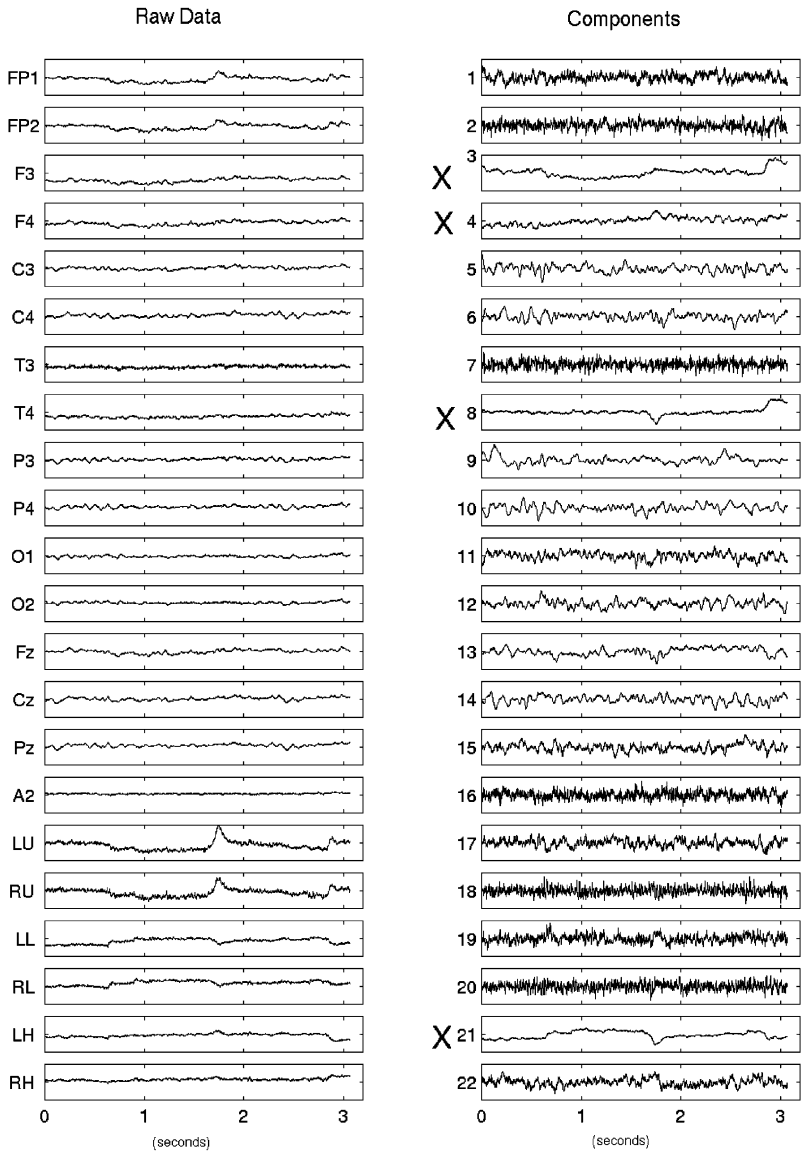

Figure 5. Column one shows preprocessed data at all recorded sites (15 EEG, 1 mastoid, 6 EOG). Column two shows the components extracted using SOBI. Components that correlate with EOG channel data (LU, RU, LL, RL, LH, RH) at 0.3 or better are marked (X) for elimination.

scaled to have a normalized amplitude value equal to 1). For this reason, small noise components in Figure 3 appear as large as eye movement components. The gain on the projection of a component onto each single electrode (i.e., how much it contributes to data recorded at that electrode) is contained in the inverse matrix, $\mathbf{W}^{-1}$, of Equation 1. Note that SOBI separates saccades (e.g., channel LH, left horizontal eye, and component "3"), as well as blink information (channel LU, left upper eye, and components "8" and "21").

Step 2. In the second step, the procedure of Step 1 is repeated, but with data from lower and horizontal EOG channels inverted with respect to the *x*-axis (i.e., multiplied by -1). The lower and horizontal EOG channels register signals generated primarily by and around the eyes (plus noise) and only weak fluctuations due to brain activity because these electrodes are located sufficiently far from the brain. For this reason, the SOBI components corresponding to those EOG specific signals that do not propagate far (noise, muscle artifact, small eye movements) become inverted with respect to their counterparts in the original component matrix obtained in Step 1 (matrix $\mathbf{S}$ of Equation 1). The decomposition of Step 2 is shown in Figure 4 with the inverted components marked by Xs on the right side of the figure. Note that upper eye channel data are not inverted, as those are likely to contain frontal cortical components that should not be inadvertently eliminated. The components that invert in Step 2 are then eliminated from matrix $\mathbf{S}$ of Equation 1.

Step 3. The components containing larger eye movements and blinks do not invert in Step 2 of the procedure because the corresponding signals propagate across the scalp and are strongly represented at many EEG electrode sites. Steps 3 and 4 work together to find these large blink and saccade components. In Step 3, the components (rows of matrix $\mathbf{S}$) from Step 1 are

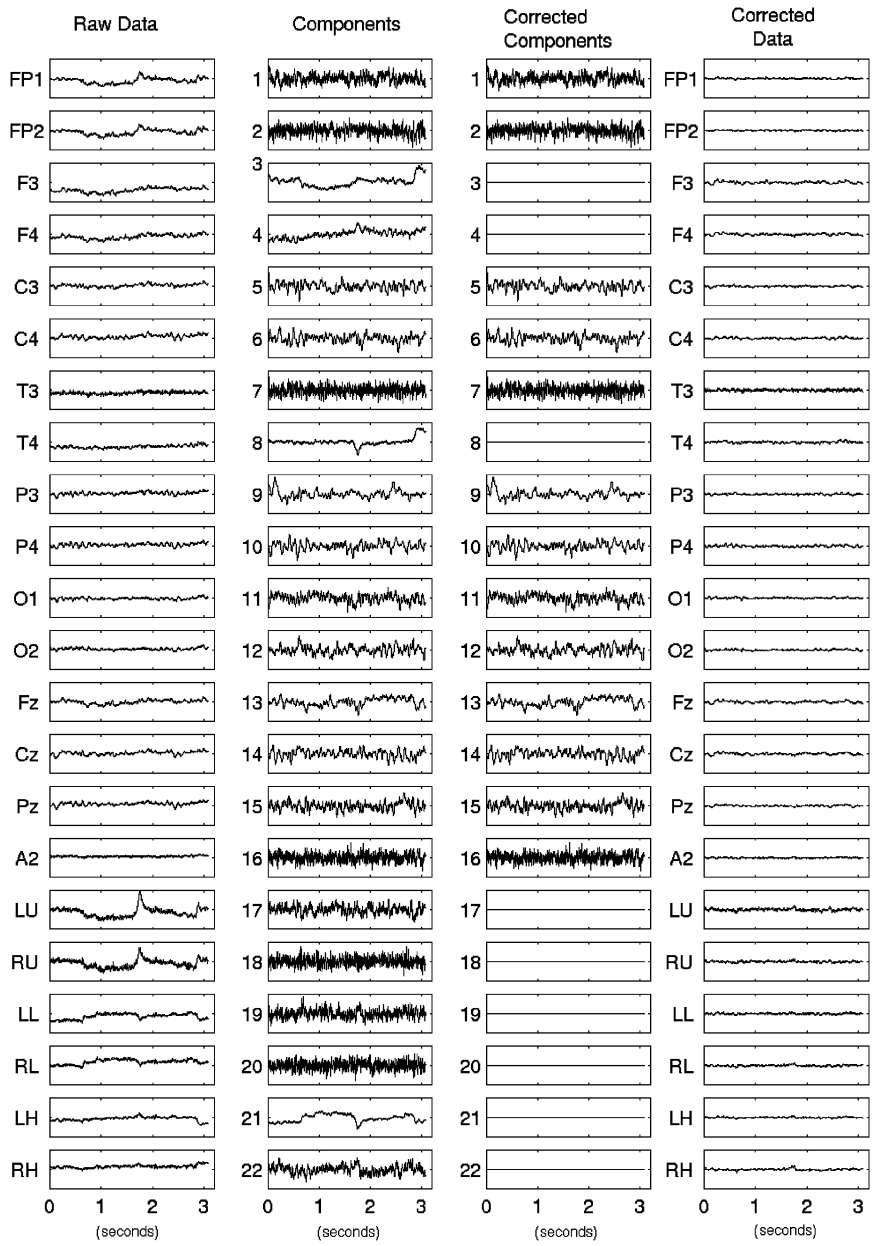

Figure 6. Column one shows the preprocessed data. Columns two and three show the components extracted by SOBI; in column three those marked for elimination have been nulled. Column four shows the corrected data recombined from the remaining components in column three and the propagation information.

correlated with the lower and horizontal EOG channel data. The idea here is that the components containing eye activity will correlate more strongly with the lower and horizontal electrode data than they will with the nonocular components because these eye electrodes reflect primarily the ocular motions and not the brain activity.

The correlation threshold level at which the component was flagged as a candidate for elimination was found as follows. As explained above, to a certain approximation, components originating in the vicinity of the eyes can be identified from the geometric relationships contained in the columns of $\mathbf{W}^{-1}$. Looking at the trials providing the cleanest separation of the ocular components, a large gap in correlation values is evident. The values were always significantly above 0.3 for SOBI components identified as originating in the vicinity of the eyes and below 0.3 for components that did not originate near the eyes. Hence the 0.3 threshold level was used in these studies to flag the SOBI components from Step 1 as shown Figure 5. However, as sampling rate can affect this relationship (these results are based on data sampled at 500 points per second), researchers should independently verify the corresponding correlation threshold level for their own data.

Step 4. The fourth step is employed to ensure that components containing nonocular, frontally generated signals, which also may correlate highly with EOG channel data, are not inadvertently eliminated. These components contain enough higher frequency brain activity that they can be distinguished

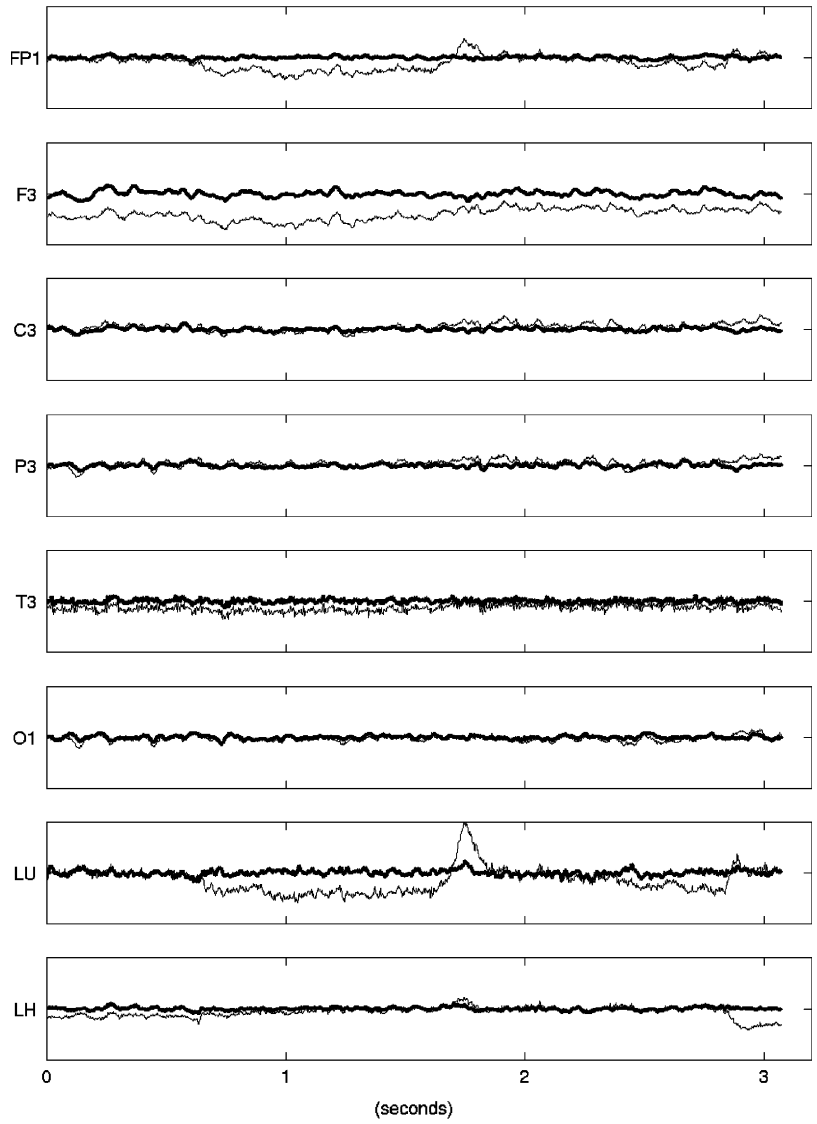

Figure 7. Corrected data is shown in the thick line and raw data in the thin line for select electrodes. Notice that corrections are largest in the EOG channels overall, largest in frontal channels for vertical contamination, and largest at the temporal channel for horizontal contamination. Notice also that there are virtually no changes at the occipital sites (small changes are due to the effects of bandpass filtering).

from ocular components using a high-pass filtering operation, as follows. The components found to correlate with lower and horizontal EOG channels at greater than 0.3 are differentiated (derivatives computed across time). If the root mean square (rms) level (standard deviation) of the derivative is low, it is an indication that the component does not contain high frequency information. As in Step 3, using very clean data separation cases, a significant gap was found at rms level 0.2 between what appeared as ocular versus frontal components. This threshold rms level (0.2) was used for final elimination of the components (Figure 6).

Step 5. In the final step, the corrected EEG data is reconstructed. All ocular components found in Step 2 and the combined output of Steps 3 and 4 are eliminated by zeroing the corresponding rows in the $\mathbf{S}$ matrix, creating $\mathbf{S}^*$, or by throwing out these rows of $\mathbf{S}$ and the corresponding columns of the $\mathbf{W}^{-1}$ matrix. The data are then reconstructed by multiplying the matrix $\mathbf{W}^{-1}$ with the corrected matrix $\mathbf{S}^*$. Figure 7 illustrates this reconstruction in which the EEG signals are preserved with no detectable EOG contamination.

Note from Figure 7 that the changes in morphology are greatest at EOG channels, and decrease from anterior to posterior electrodes with little or no change at occipital sites. This correction is consistent with how eye movement signals propagate across the scalp. Occasionally changes in morphology at posterior electrode sites are caused by the procedure. This appears to occur in cases where there is some drift in all electrodes, implicating drift at the reference site. Because this drift is as highly correlated with eye channels as with EEG channels, and contains mainly low frequencies, it is eliminated by the procedure. This is in fact desirable. Channel drift and noise generated at EOG electrodes are also eliminated by this method.

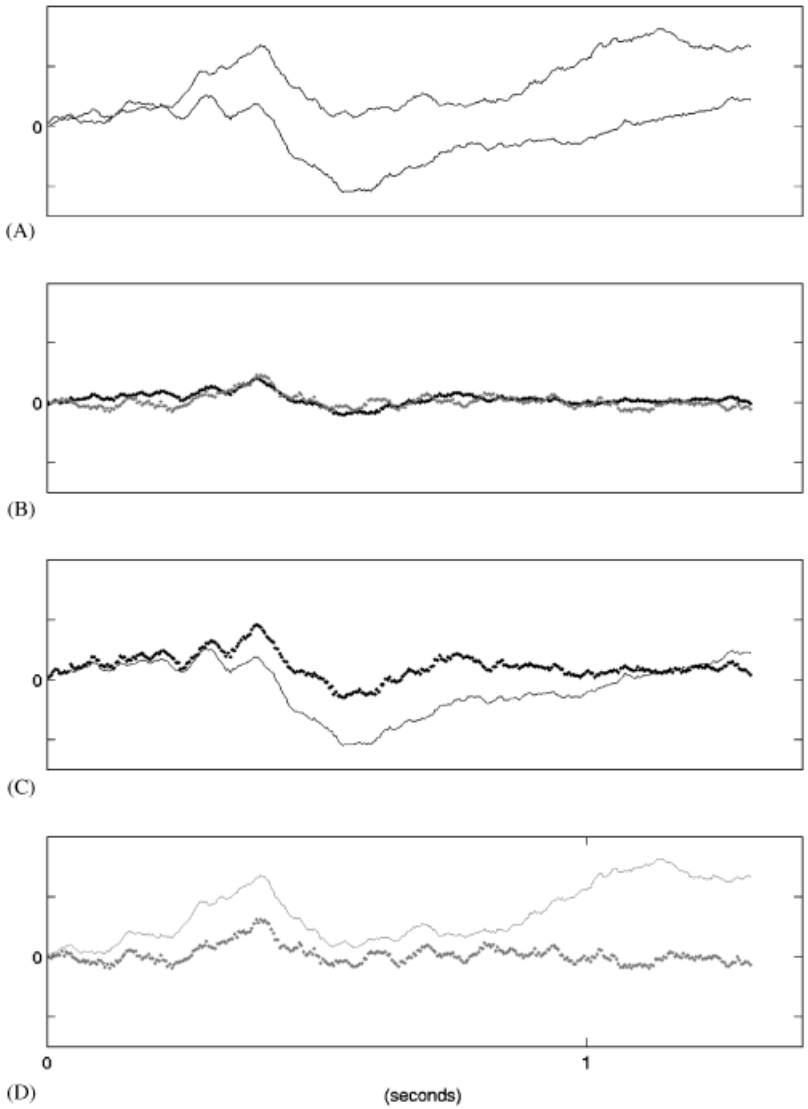

Figure 8. A: An average of 100 EOG artifact-free trials (black thin line) is plotted against an average of 100 trials containing ocular and drift artifacts (gray thin line). B: Those same 100 trial averages are plotted after application of the EOG correction procedure to each trial (thick black line = EOG artifact free, thick gray line = artifacts). Note that there is even some small change to the EOG artifact-free trials due to the DC correction procedure and the fact that the EOG correction procedure eliminates some drift artifact as well. C: The EOG artifact-free averages before (thin line) and after (thick line) correction. D: The EOG contaminated averages before (thin line) and after (thick line) correction. The data are from a midline frontal electrode site (FZ), courtesy of Tom Urbach and Marta Kutas.

Figure 8 illustrates another example using averaged data. Averages of 100 artifact-free trials and 100 trials containing ocular artifacts taken from the same individual within the same experimental paradigm are shown both prior to and following application of the EOG correction procedure. Note two things: (1) the averages containing the artifact-free trials are relatively unaffected by the correction procedure (other than some general drift correction), and (2) the average of the contaminated trials following correction is virtually identical to the average of the artifact-free trials.

Discussion

This article presents a procedure for automated correction of ocular artifacts in EEG records using blind source separation and correlation metrics. The methodology can open many doors for investigators to allow more natural, free viewing of stimuli in ERP studies. The technique presented here can be extended to eliminate certain other sources of artifacts as well. Electrode drift and electrocardiac signals can be addressed in a straightforward manner by this approach albeit using different tuning parameters to classify the signals based on their specific characteristics. Vocalization and cranial muscle movement artifacts are similar to EOG artifacts and thus also can be removed by adapting the present technique provided electrodes are placed where signals from these artifacts can be captured. Currently these artifacts are dealt with by discarding contaminated trials. Other types of artifacts, such as small muscle spasms, may be best addressed by different data filtering approaches. Small muscle activity, for example, tends to saturate single

rather than distributed electrode sites. BSS-based approaches, thus, may not be ideal for detection of muscle-related components in this situation; analysis and filtering of raw potential values at individual electrode sites may be a better approach for this type of noise.

As discussed earlier, the key to assuring that the BSS components cleanly capture the artifact signals and separate them from the components of brain activity is to choose a BSS algorithm whose underlying assumptions most closely match the physical properties of the problem at hand. Such considerations are necessary because BSS solutions cannot be validated by directly measuring the activity at individual sites in the head. SOBI's ability to separate correlated signals is one reason for the differences in the observed performance of SOBI versus the ICA algorithms and the primary reason it was chosen for the current procedure. SOBI offers a number of additional favorable properties worth reviewing here. SOBI uses averaged statistics across time, perhaps the second most powerful feature of this algorithm and the most undervalued one. The average statistics means that errors due to noise in SOBI components are averaged across time. Hence, the components are much less sensitive to random noise in the data than are algorithms that use instantaneous statistics derived from individual time points. This is important in the low signal-to-noise environment typical of EEG data.

Another advantage of SOBI is that it uses only second-order statistics that can be estimated reliably with significantly fewer data points than the fourth- and higher-order statistics used in ICA algorithms. This means that short segments of data are sufficient for estimating SOBI components. Segments as short as 100 data points worked well with SOBI, whereas the ICA-type algorithms tested required an order of magnitude more data points. This becomes important when dealing with activity whose statistical properties may vary even moderately over time, in other words, when the sources are not guaranteed to be stationary. The fourth important reason for selecting SOBI is that it can separate Gaussian sources. A major shortcoming of the ICA algorithms is their failure to separate more than one Gaussian or near-Gaussian source. Because the actual probability distributions of EEG sources cannot be measured, it is not known how common Gaussian distributions may be, but evidence to assume otherwise at this point is lacking. SOBI allows this issue to be sidestepped altogether. Besides these four major considerations for selecting SOBI for ocular artifact correction, there are a number of minor considerations that come into play when choosing between BSS algorithms. For example, some ICA algorithms assume temporal whiteness of the signal components. In general, the assumptions depend on the particulars of the individual algorithms and their implementations; however, a complete review of these is outside the scope of this article. One shortcoming of SOBI was observed in the evaluation. SOBI is limited in separating out short-duration signals such as eyeblinks. In this study, SOBI frequently integrated the blink into the eye movement component; thus, the eyeblink component could be extracted with the rest of ocular activity. In other cases, however, the blink component would appear, somewhat weakly, in some of the nonocular components. Nonetheless, overall, SOBI performance stood apart from the rest of the algorithms and, based on this, SOBI was chosen for this procedure.

The discussion above is meant to heighten the awareness that BSS algorithms are not expected to produce physically meaningful components unless their underlying assumptions present a good fit to the signal properties being estimated. Thus, interpretation of BSS results must be carried out with care. Further improvements to BSS methods for EEG analysis are clearly desirable. An algorithm that combines, in an averaging sense, the metrics used by SOBI and by ICA and which to a large extent overcomes the reviewed shortcomings of the ICA and the SOBI algorithms while preserving their advantages was developed in Gorodnitsky and Belouchrani (2001). In the initial investigation, this algorithm was found to perform better than the current BSS methods in identifying ocular artifacts, but it was not completely validated at the time this report was written. As more accurate algorithms develop, more direct procedures to identify artifacts using their points of origination can be implemented. Further, using advanced classification methods to identify components containing artifacts is also promising.

REFERENCES

Achim, A., Richer, F., & Saint-Hilaire, J. (1991). Methodological considerations for the evaluation of spatio-temporal source models. *Electroencephalography and Clinical Neurophysiology*, *79*, 227–240.

Belouchrani, A., Abed-Meraim, K., Cardoso, J. F., & Moulines, E. (1993). Second-order blind source separation of correlated sources. *Proceedings of the International Conference on Digital Signal Processing* (pp. 346–351). Available at: http://cloe.ucsd.edu/adel/.

Belouchrani, A., Abed-Meraim, K., Cardoso, J. F., & Moulines, E. (1997). A blind source separation technique using second-order statistics. *IEEE Transactions on Signal Processing*, *45*, 434–444.

Berg, P., & Scherg, M. (1991a). Dipole models of eye movements and blinks. *Clinical Neurophysiology*, *79*, 36–44.

Berg, P., & Scherg, M. (1991b). Dipole modeling of eye activity and its application to the removal of eye artifacts from the EEG and MEG. *Clinical Physiology and Physiological Measurements*, *12*(A), 49–54.

Berg, P., & Scherg, M. (1994). A multiple source approach to the correction of eye artifacts. *Electroencephalography and Clinical Neurophysiology*, *90*, 229–241.

Cardoso, J.-F., & Souloumiac, A. (1993). Blind beamforming for non-Gaussian signals. *IEEE Proceedings-F*, *140*, 362–370.

Delorme, A., Makeig, S., & Sejnowski, T. (2001). Automatic artifact rejection for EEG data using high-order statistics and independent component analysis. *Proceedings of the Third International ICA Conference, December 9–12, San Diego*. Available at: http://www.sccn.ucsd.edu/~arno/indexpubli.html.

Gorodnitsky, I. F., & Belouchrani, A. (2001). Joint cumulant and correlation based signal separation with application to EEG data analysis. *Proceedings of the Third International ICA Conference, December 9–12, San Diego*. Available at: http://cloe.ucsd.edu/BSS-validation.html.

Gratton, G. (1998). Dealing with artifacts: The EOG contamination of the event-related brain potential. *Behavior Research Methods, Instruments, & Computers*, *30*, 44–53.

Hyvarinen, A., & Oja, E. (1997). A fast fixed-point algorithm for independent component analysis. *Neural Computation*, *9*, 1483–1492.

Joyce, C. A., Gorodnitsky, I., King, J. W., & Kutas, M. (2002). Tracking eye fixations with electroocular and electroencephalographic recordings. *Psychophysiology*, *39*, 607–618.

Joyce, C. A., Gorodnitsky, I. F., Teder-Sälejärvi, W. A., King, J. W., & Kutas, M. (2002). Variability in AC amplifier distortions: Estimation and correction. *Psychophysiology*, *39*, 633–640.

Jung, T., Makeig, S., Humphries, C., Lee, T., McKeown, M. J., Iragui, V., & Sejnowski, T. J. (2000). Removing electroencephalographic artifacts by blind source separation. *Psychophysiology*, *37*, 163–178.

Lee, T. W., Girolami, M., & Sejnowski, T. J. (1999). Independent component analysis using an extended infomax algorithm for mixed sub-Gaussian and super-Gaussian sources. *Neural Computation*, *11*, 417–441.

Lins, O. G., Picton, T. W., Berg, P., & Scherg, M. (1993a). Ocular artifacts in EEG and event-related potentials, I: Scalp topography. *Brain Topography*, *6*, 51–63.

Lins, O. G., Picton, T. W., Berg, P., & Scherg, M. (1993b). Ocular artifacts in recording EEGs and event-related potentials, II: Source dipoles and source components. *Brain Topography*, *6*, 65–78.

Overton, D. A., & Shagass, C. (1969). Distribution of eye movement and eyeblink potentials over the scalp. *Electroencephalography and Clinical Neurophysiology*, *27*, 546.

Sadasivan, P. K., & Dutt, D. N. (1996). SVD based technique for noise reduction in electroencephalographic signals. *Signal Processing*, *55*, 179–189.

Tang, A. C., Pearlmutter, B. A., Malaszenko, N. A., Phung, D. B., & Reeb, B. C. (2002). Independent components of magnetoencephalography: Localization. *Neural Computation*, *14*, 1827–1858.

Vigario, R. N. (1997). Extraction of ocular artefacts from EEG using independent component analysis. *Electroencephalography and Clinical Neurophysiology*, *103*, 395–404.

(Received November 4, 2002; Accepted July 13, 2003)